

# ENSURE: A general approach for unsupervised training of deep image reconstruction algorithms

Hemant Kumar Aggarwal, *Member, IEEE*, Aniket Pramanik, Mathews Jacob, *Senior Member, IEEE*

**Abstract**—Image reconstruction using deep learning algorithms offers improved reconstruction quality and lower reconstruction time than classical compressed sensing and model-based algorithms. Unfortunately, clean and fully sampled ground-truth data to train the deep networks is often not available in several applications, restricting the applicability of the above methods. This work introduces the Ensemble Stein’s Unbiased Risk Estimate (ENSURE) framework as a general approach to train deep image reconstruction algorithms without fully sampled and noise-free images. The proposed framework is the generalization of the classical SURE and GSURE formulation to the setting where the images are sampled by different measurement operators, chosen randomly from a set. We show that the ENSURE loss function, which only uses the measurement data, is an unbiased estimate for the true mean-square error. Our experiments show that the networks trained with this loss function can offer reconstructions comparable to the supervised setting. While we demonstrate this framework in the context of MR image recovery, the ENSURE framework is generally applicable to arbitrary inverse problems.

**Index Terms**—Unsupervised Learning, Inverse Problems, Deep Learning, SURE, MRI.

## I. INTRODUCTION

The recovery of images from a few of their noisy measurements is a classical inverse problem, which is central to several imaging modalities. For instance, the recovery of MR images from a few of their multi-channel k-space samples using compressed sensing (CS) [1]–[3] algorithms is a popular approach to speed up the scans. A central challenge with CS algorithms that rely on iterative algorithms is the high computational complexity. Recently, deep learning methods have been emerging as powerful alternatives to CS-based approaches. These methods rely on convolutional neural network (CNN) models that offer reduced computational complexity and improved performance. Many of the current approaches directly learn an inverse mapping from undersampled measurements to images [4], [5]. Model-based approaches, which account for the imaging physics using a numerical model along

with a deep learned prior, are also emerging. These model-based approaches unroll an iterative algorithm to minimize the cost function, whose deep modules are learned in an end-to-end fashion [6]–[11]. Most of the above approaches are supervised algorithms. They rely on large quantities of fully sampled training data to train the deep learning modules. While large multi-center datasets are emerging for common applications such as brain and knee imaging [12], similar datasets are not available in many applications. More importantly, it is often challenging to acquire fully sampled datasets in applications including dynamic and static MRI with high spatial and temporal resolution. Unsupervised methods that can learn the deep networks from undersampled data directly can significantly improve the applicability of these approaches.

The unsupervised optimization of the parameters of image reconstruction and denoising algorithms have a long history. Early approaches relied on L-curve [13] and generalized cross-validation [14] to optimize the regularization parameters in regularized image recovery. Another approach is to use the Stein’s Unbiased Risk Estimate (SURE) [15] to determine the optimal parameters. The SURE loss is an unbiased estimate of the mean-square-error (MSE) that only depends on the recovered image and the noisy measurements. For example, SURE-let- and PURE-let-based methods optimize the thresholds in wavelet-based image denoising with Gaussian [16], [17] and Poisson noise [18]. Recently, SURE has been used to train deep image denoisers in [19]–[21]. Other unsupervised strategies have recently been introduced to train deep image denoisers. For instance, the Noise2Noise [22] approach relies on a pair of noisy images to train a denoiser without the need for clean images, which are not available in many applications, including microscopy. To avoid the need for paired measurements, the Noise2Void [23] approach was introduced. This is a blind spot method that excludes the central pixel from the network’s receptive field.

The SURE approach was extended to inverse problems with a rank-deficient measurement operator, which is termed as generalized SURE (GSURE) [24]. The GSURE provides an unbiased estimate of the projected MSE, which is the expected error of the projections in the range space of the measurement operator. The GSURE approach was recently used for inverse problems in [19]. Unfortunately, the experiments in [19] show that the GSURE-based projected MSE is a poor approximation of the actual MSE in the highly undersampled setting. To improve the performance, the authors trained the denoisers at each iteration in a message-passing algorithm in a layer-by-

Hemant Kumar Aggarwal (email: hemantkumar-aggarwal@uiowa.edu), Aniket Pramanik (email: aniket-pramanik@uiowa.edu), and Mathews Jacob (email: mathews-jacob@uiowa.edu) are with the Department of Electrical and Computer Engineering, University of Iowa, Iowa, USA, 52242.

Manuscript received Month day, year; revised Month day, year.

This work is supported by 1R01EB019961-01A1 and 1R01AG067078-01A1. This work was conducted on an MRI instrument funded by 1S10OD025025-01.

layer fashion using classical SURE, which is termed LDAMP-SURE [19]. This approach approximates the residual aliasing errors at each iteration to be Gaussian random noise. A similar approach was used for MRI recovery in [21].

In the supervised context, the end-to-end training of model-based algorithms [6]–[11] have been shown to be significantly more efficient than the layer-by-layer training strategies [19], [21]. Unfortunately, the end-to-end unsupervised learning of model-based deep image reconstruction algorithms is challenging in the highly undersampled setting [19], [25], [26], mainly because the measurements only offer a fraction of the image information. The deep image prior (DIP) approach [27] was introduced for unsupervised learning in ill-posed settings. DIP relies on the structured bias of CNN modules towards images as an implicit regularization in the undersampled setting. However, this approach requires the learning of the CNN for each image, resulting in high computational complexity. In addition, the quality of the images recovered by DIP is often not as good as the ones obtained by supervised training. Recently, the self-supervised learning using data undersampling (SSDU) approach, which has conceptual similarities to the blind-spot-based method [23], was introduced for the end-to-end training of unrolled algorithms. This approach partitions the measured k-space into two disjoint sets. The first set is used in the data consistency step, and the remaining set is used for measuring the error. SSDU also uses different sampling operators for each image to improve the diversity of the observed k-space samples. This approach is more effective than using all the k-space measurements for data consistency and evaluating the error.

We introduce a novel loss function termed as ensemble Stein's Unbiased Risk Estimate (ENSURE). Similar to [25], we use different sampling operators for different images. We note that such a measurement scheme can be realized in practice, where a different sampling mask can be chosen from a lookup table for each image. We introduce a SURE-based loss function for training deep networks, assuming that the sampling operator for each image is randomly chosen from a set. Similar to classical SURE metrics [16], [24], the proposed ENSURE loss metric has a data consistency term and a divergence term. The divergence term is similar to the GSURE setting. By contrast, the data consistency term in ENSURE is the sum of the weighted projected losses [24]; the weighting depends on the class of sampling operators. We show that ENSURE is an unbiased estimate for the true image MSE and hence is a superior loss function than projected SURE [24] to train deep image reconstruction algorithms. When the divergence term is not used, the proposed loss reduces to only the projection error, which is observed to offer poor performance. The divergence term serves as a network regularization that minimizes the over-fitting to the measurement noise. The experiments demonstrate that the proposed ENSURE approach can offer results comparable to supervised training.

## II. BACKGROUND

In this section, we briefly review the background to make the paper self-contained.

### A. Inverse Problems & Supervised Learning

We consider the acquisition of the complex-valued image  $\rho \in \mathbb{C}^N$  using the multichannel measurement operator  $\mathcal{A}_s$  as

$$\mathbf{y}_s = \mathcal{A}_s \rho + \mathbf{n}. \quad (1)$$

We assume the noise  $\mathbf{n}$  to be Gaussian distributed with zero mean and covariance matrix  $\mathbf{C}$  such that  $\mathbf{n} \sim \mathcal{N}(0, \mathbf{C})$ . We note that the probability distribution function (PDF) of  $\mathbf{y}_s$  is given by  $p(\mathbf{y}_s | s) = \mathcal{N}(\mathcal{A}_s \rho, \mathbf{I})$ .

We assume the measurement operator  $\mathcal{A}_s$  to be randomly chosen and parameterized by a random vector  $s$  that is independent from  $\mathbf{n}$ , drawn from a set  $\mathcal{S}$ . In the MRI setting, the vector  $s$  can be viewed as the k-space sampling mask, where the probability of observing a specific sample could depend on the k-space location. We note that such a model could account for variable density masks used in MRI. The goal of the image reconstruction scheme is to recover  $\rho$  from  $\mathbf{y}_s$ . The inverse problem in (1) gets simplified to the image denoising model when  $\mathcal{A}_s = \mathcal{I}$ .

Supervised deep learning methods learn to recover the fully sampled image  $\hat{\rho}$  only from noisy and undersampled measurements  $\mathbf{y}_s$ . Let

$$\mathbf{u} = \mathcal{A}_s^H \mathbf{y}_s \quad (2)$$

be the zero-filled reconstruction. We note that  $\mathbf{u}$  is a random variable because of the additive noise in (1). In that case, the recovery using a deep neural network  $f_\Phi$  with trainable parameters  $\Phi$  is represented as

$$\hat{\rho} = f_\Phi(\mathbf{u}). \quad (3)$$

Here  $f_\Phi$  can be a direct-inversion or a model-based deep neural network. Supervised approaches often rely on the loss function:

$$\text{Sup-Loss} = \sum_{i=1}^{N_{\text{train}}} \|\hat{\rho}_i - \rho_i\|_2^2 \quad (4)$$

to train the network using  $N_{\text{train}}$  number of images.

### B. Unsupervised Learning of Denoisers

When noise-free training data is unavailable, denoising approaches such as Noise2Noise [22] and blind-spot methods [23], [25], [28] have been introduced for unsupervised learning of the network parameters  $\Phi$ . Assuming the additive noise  $\mathbf{n}$  to be Gaussian distributed, the SURE [15] approach uses the loss function

$$\text{SURE}(\hat{\rho}, \mathbf{u}) = \|\hat{\rho} - \mathbf{u}\|_2^2 + 2\sigma^2 \nabla_{\mathbf{u}} \cdot f_\Phi(\mathbf{u}) - N\sigma^2, \quad (5)$$

which is an unbiased estimate of the true mean-square error, denoted by

$$\text{MSE} = \mathbb{E}_{\mathbf{u}} \|\hat{\rho} - \rho\|^2 \quad (6)$$

Note that the expression in (5) does not depend on the noise-free images  $\rho$ ; it only depends on the noisy images  $\mathbf{u}$  and the estimates  $\hat{\rho}$ . In (5),  $\nabla_{\mathbf{u}} \cdot f_\Phi(\mathbf{u})$  represents network divergence, which is often estimated using Monte-Carlo simulations [29]. Several researchers have adapted SURE as a loss function for the unsupervised training of deep image denoisers [19], [21] with performance approaching that of supervised methods.

### C. Unsupervised training with rank deficient $\mathcal{A}$

The unsupervised training of deep networks for image recovery is significantly more challenging than the denoising setting, when  $\mathcal{A}$  is rank deficient. In particular, the measurement model only acquires partial information about the images, in addition to the additive noise. The DIP [27] approach exploits the structural bias of CNNs towards natural images; they optimize the network parameters such that the loss  $\|\mathcal{A}_s \hat{\rho} - \mathbf{y}_s\|_2^2$  is minimized. Since this approach requires the network to be trained for each image, the computational complexity is high during inference. In addition, the quality of the recovered images is often inferior to the ones obtained from supervised training. Another challenge is the need for manual early stopping of the algorithm to minimize the over-fitting to noise.

One may use the generalization of a DIP approach for an ensemble of images, which we term as measurement domain (k-space in MRI) MSE loss:

$$\text{K-MSE} = \sum_{i=1}^{N_{\text{train}}} \|\mathcal{A}_{s_i} \hat{\rho}_i - \mathbf{y}_{s_i}\|_2^2. \quad (7)$$

This K-MSE approach is prone to over-fitting the reconstructed image to the noisy measurements [25]. The SSDU approach [25] was introduced to minimize this over-fitting [25]. SSDU, which may be viewed as an extension of blind-spot methods (e.g., [23]), suggests partitioning the available k-space into two disjoint groups for the data-consistency step and loss function estimation, respectively. The partitioning of k-space, along with the use of different sampling masks for different images, is observed to provide improved results when compared to (7).

The projected GSURE approach was used to train model-based deep learning algorithms in the unsupervised setting in [19]. Specifically, the GSURE loss is an unbiased estimate of the projected MSE

$$\text{MSE}_s = \mathbb{E}_{\rho \sim \mathcal{I}} \|\mathbf{P}_s (\hat{\rho} - \rho)\|^2, \quad (8)$$

where  $\mathbf{P}_s = \mathcal{A}_s^H (\mathcal{A}_s \mathcal{A}_s^H)^{-1} \mathcal{A}_s$  is the projection operator to the range space of  $\mathcal{A}_s^H$ . The authors of [19] noted that  $\text{MSE}_s$  is a poor approximation of MSE in the highly undersampled setting. Hence, instead of directly using GSURE, the LDAMP algorithm instead relies on layer-by-layer training of deep learned denoisers [19] using the SURE loss discussed in Section II-B. This scheme implicitly assumes that the alias artifacts at each iteration are Gaussian distributed, which is not a realistic assumption. In addition, the end-to-end training of model-based algorithms [6]–[9] often offers improved performance compared to the above layer-by-layer strategies.

### III. ENSEMBLE SURE (ENSURE) FRAMEWORK

The training of the deep network  $f_\Phi$  in (3) using only the measurements  $\mathbf{y}_s$  in (1) is challenging when the sampling operator  $\mathcal{A}_s$  is rank deficient. More specifically,  $\mathbf{y}_s$  carries only partial information about the images  $\rho$ , in addition to being noisy. To overcome the poor approximation of the MSE by  $\text{MSE}_s$ , we consider the sampling of each image by a different sampling operator. In the MRI context, we assume the k-space sampling mask  $s$  to be a random vector drawn from

the distribution  $S$ . Note that this acquisition scheme is realistic and can be implemented in many applications. For instance, it may be difficult to acquire a specific image in a fully sampled fashion due to time constraints. However, one could use a different undersampling mask for each image  $\rho \sim \mathcal{I}$ . We note that such a framework is assumed in [25].

#### A. Direct extension of GSURE

We first show that the direct extension of the GSURE framework, which approximates the projected MSE, to the setting with multiple images and different sampling operators is undesirable. We consider a specific image  $\rho$  and consider the expectation of the projected MSE over an ensemble of measurement operators:

$$\mathcal{Q}(u) = \mathbb{E}_u \left[ \mathbb{E}_{s \sim S} \left[ \|\mathbf{P}_s (\hat{\rho} - \rho)\|^2 \right] \right]. \quad (9)$$

We note that this measure depends on the true image  $\rho$  and hence cannot be directly computed in the unsupervised setting. The following result shows that the above measure only gives a weighted version of the true MSE in (6).

*Lemma 1:* The expected loss  $\mathcal{Q}$  in (9) is equal to the weighted MSE:

$$\mathcal{Q} = \mathbb{E}_u \left[ \|\mathbf{W} (\hat{\rho} - \rho)\|^2 \right], \quad (10)$$

where  $\mathbf{W}$  is a weighting matrix that is dependent on the set of measurement operators.

*Proof:* Denoting the error  $e = \hat{\rho} - \rho$  and ignoring its dependence on  $s$ , we obtain

$$\mathcal{Q} = \mathbb{E}_u \left[ \mathbb{E}_s \left[ \|\mathbf{P}_s e\|^2 \right] \right] \quad (11a)$$

$$\approx \mathbb{E}_u \left[ e^T \mathbb{E}_s [\mathbf{P}_s] e \right] = \mathbb{E}_u \left[ e^T \mathbf{Q} e \right] \quad (11b)$$

We used the symmetry of the projection operators and  $\mathbf{P}^2 = \mathbf{P}$  in the above step. Here,  $\mathbf{Q}$  is the ensemble of projection operator. We denote the matrix square root of  $\mathbf{Q}$  by  $\mathbf{W}$  (i.e.,  $\mathbf{W}^2 = \mathbf{Q}$ ) to obtain

$$\mathcal{Q} = \mathbb{E}_u \left[ e^T \mathbf{W}^T \mathbf{W} e \right] \quad (11c)$$

$$= \mathbb{E}_u \left[ \|\mathbf{W} (\hat{\rho} - \rho)\|_2^2 \right], \quad (11d)$$

Note that the  $\mathbf{Q}$  corresponds to the average of the projection operators. Depending on the sampling operators, the weighting by  $\mathbf{W}$  amounts to weighting some aspects of the images more heavily than other features.

We will now illustrate the above result in the special case of single-channel MRI, when  $\mathcal{A}_s = \mathbf{S}\mathbf{F}$ , where  $\mathbf{F}$  is the Fourier matrix and  $\mathbf{S}$  is the sampling matrix. The projection  $\mathbf{P}_s$  gets simplified as  $\mathbf{P}_s = \mathcal{A}_s^H (\mathcal{A}_s \mathcal{A}_s^H)^{-1} \mathcal{A}_s = \mathbf{F}^H \mathbf{M}_s \mathbf{F}$ . Here,  $\mathbf{M}_s = \text{diag}(\mathbf{m})$  is a diagonal matrix. The entries  $\mathbf{m}_i$  are one if the specific sample is acquired and zero otherwise.

We now consider the entries  $\mathbf{m}_i$  to be drawn from a Bernoulli distribution with a probability  $d_i$  that depends on the spatial location. Note that variable-density masks are routinely

used in CS settings. We thus obtain  $\mathbf{Q} = \mathbf{F}^H \text{diag}(\mathbf{d}) \mathbf{F}$ , which translates to

$$\mathbf{W} = \mathbf{F}^H \text{diag}(\sqrt{\mathbf{d}}) \mathbf{F} \quad (12)$$

The weighted loss  $\mathcal{Q}$  is equivalent to the MSE if the sampling density is uniform. However, most sampling operators rely on variable-density masks with higher density in the k-space center. In this case, the training of the networks using  $\mathcal{Q}$  will translate to reduced weighting for higher Fourier samples, resulting in reduced high-frequency details.

### B. ENSURE: Unbiased Estimate of MSE

We observe that the direct extension of the projected MSE to the setting with an ensemble of sampling masks is not desirable due to the weighting. To compensate for this distortion, we now consider the weighted version of the projected MSE:

$$\mathcal{L} = \mathbb{E}_{\mathbf{u}} \left[ \mathbb{E}_{\mathbf{s} \sim \mathcal{S}} \left[ \|\mathbf{R}_s(\hat{\rho} - \rho)\|_2^2 \right] \right], \quad (13)$$

where  $\mathbf{R}_s = \mathbf{W}^{-1} \mathbf{P}_s$  is the weighted projection operator. We note that  $\mathbf{R}_s \rho$  still lives in the range space of  $\mathcal{A}$ . Using a similar argument in Lemma 1, we can show that  $\mathcal{L} = \text{MSE}$ . This approach thus opens a way to evaluate the MSE using only the measurements.

We note that the loss functions (13) and (10) depend on the fully sampled ground truth images  $\rho_i; i = 1, \dots, N$ . Hence, it is impossible to directly compute it in an unsupervised setting. We hence approximate it by its unbiased estimate, which we call ENSURE. We define the ENSURE loss as

$$\text{ENSURE} = \frac{1}{N} \sum_{i=1}^N \left( \underbrace{\|\mathbf{R}_{s_i}(\hat{\rho}_i - \rho_{LS,i})\|_2^2}_{\text{dataterm}} + \underbrace{\nabla_{\mathbf{u}_i} \cdot \mathbf{f}_{\Phi}(\mathbf{u}_i)}_{\text{divergence}} \right) + \kappa \quad (14)$$

Here,  $\mathbf{u}_i = \mathcal{A}_{s_i}^H \mathbf{y}_i$ ,  $\kappa$  is a constant, and  $\rho_{LS,i}$  is the least-squares solution specified by

$$\rho_{LS} = (\mathcal{A}_s^H \mathcal{A}_s)^{\dagger} \mathcal{A}_s^H \mathbf{y}_s. \quad (15)$$

Here,  $\nabla_{\mathbf{u}}$  represents the divergence of the network  $f_{\Phi}$  with respect to its input  $\mathbf{u}$ .

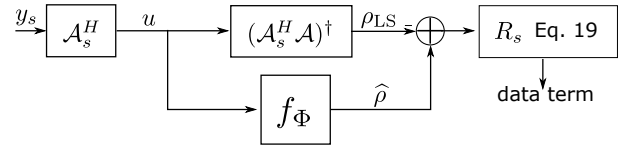
We note that the ENSURE loss function can be computed without knowing the fully sampled and noise-free images. The data term in (14) involves the average of the weighted projected losses evaluated over the  $N$  training examples. The divergence term is computed over all the data without worrying about the sampling patterns.

We now state our main result below, which shows that ENSURE is an unbiased estimate for the MSE in (6).

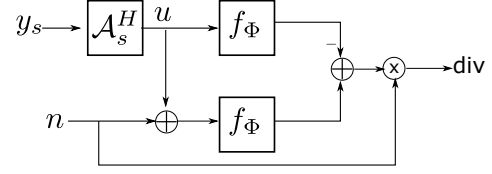
**Lemma 2:** The ENSURE loss specified by (14) is an unbiased estimate for the MSE. Specifically, we have

$$\mathbb{E}_{\rho \in \mathcal{I}} [\mathbb{E}_{\mathbf{s} \in \mathcal{S}} [\text{ENSURE}]] = \text{MSE}(\rho) \quad (16)$$

Please see the appendix for the proof of the above result. Based on the above result, we propose to use the ENSURE loss function to train the model-based image recovery algorithm.



(a) Data-term in Lemma 2



(b) Divergence in Lemma 2

Fig. 1. Visual representation of the computation of the data and divergence terms in the proposed ENSURE estimate in (14). Here,  $\oplus$  and  $\otimes$  represent the addition and inner-product, respectively.

### C. Implementation details

We compute the least-squares solution in (15) as

$$\rho_{LS} = \arg \min_{\rho} \|\mathcal{A}_s \rho - \mathbf{y}_s\|^2 + \lambda \|\rho\|^2 \quad (17)$$

with  $\lambda \rightarrow 0$ . In the MRI setting,  $\rho_{LS,s}$  is often called the SENSE [30] solution. We compute the projection operator  $\mathbf{P}_s = (\mathcal{A}_s^H \mathcal{A}_s)^{\dagger} (\mathcal{A}_s^H \mathcal{A}_s)$  in (9) and (14) as

$$\mathbf{P}_s \mathbf{e} = \arg \min_{\zeta} \|\mathcal{A}_s \zeta - \mathcal{A}_s \mathbf{e}\|^2 + \lambda \|\rho\|^2 \quad (18)$$

with  $\lambda \rightarrow 0$ ; in the MRI setting, this corresponds to the SENSE recovery from  $\mathcal{A}_s \mathbf{e}$ . When the weighting is also included, we compute

$$\mathbf{R}_s \mathbf{e} = \arg \min_{\zeta} \|\mathbf{D}_s \mathcal{A}_s (\zeta - \mathbf{e})\|^2 + \lambda \|\rho\|^2, \quad (19)$$

where  $\mathbf{D}_s = \text{diag}(\mathbf{d}_s^{-\frac{1}{2}})$ , where  $\mathbf{d}_s$  corresponds to the density at the sampling locations.

Combining (17) and (19), the computational structure of the data term is shown in Fig. 1(a). In particular, we compare the recovered images with their CG-SENSE reconstructions specified by  $\rho_{LS}$ . Note that the CG-SENSE solutions may have residual aliasing components. To make the data consistency term insensitive to these errors, the error  $\mathbf{e} = \hat{\rho} - \rho_{LS}$  is projected to the range space of  $\mathcal{A}_s$ . An additional weighting is used to compensate for the non-uniform density of the sampling patterns in k-space, which is implemented as in (19).

The divergence term in (14) is computed using Monte-Carlo simulations [29] as in Fig. 1(b). Specifically, noise perturbations are added to the input to the network, and the corresponding perturbations in the output of the network are estimated. The divergence term is approximated as

$$\text{div}_u(f_{\Phi}(u)) = \lim_{\epsilon \rightarrow 0} \frac{1}{\epsilon} \mathbb{E}_n \left[ \mathbf{n}^T (f_{\Phi}(\mathbf{u}_s + \epsilon \mathbf{n}) - f_{\Phi}(\mathbf{u}_s)) \right].$$

Here  $\mathbf{n}$  is the standard Gaussian. As in [29], we observe that the expectation can be approximated by a Monte-Carlo approach involving different noise realizations. In practice, one noise realization per image per epoch is sufficient to obtain a good approximation as observed in [29]. Note that the



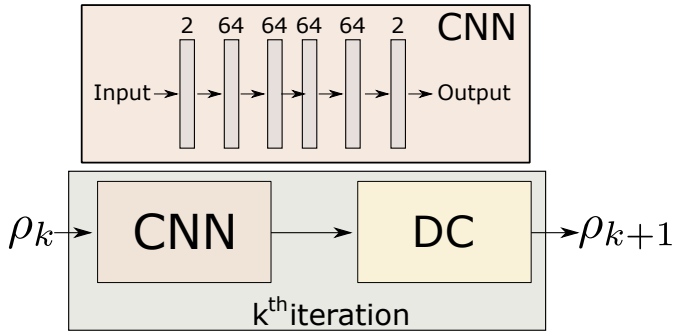


Fig. 2. The specific network architecture used in the experiments. The CNN is a five-layer model that takes complex data as input. Each of the middle layers has 64 feature maps. It concatenates real and imaginary components as channels in the first layer. Similarly, the last layer output is converted to the complex type before it enters the data-consistency (DC) step.

TABLE I

QUANTITATIVE COMPARISON OF PSNR (DB) AND SSIM VALUES. EACH VALUE SHOWS MEAN  $\pm$  STD.

acceleration	Peak Signal to Noise Ratio (PSNR)		
	4x	4x, $\sigma = 0.03$	6x
E-to-E-Sup	37.71 $\pm$ 0.97	35.34 $\pm$ 0.70	35.39 $\pm$ 0.92
L-by-L-Sup	36.64 $\pm$ 1.07	35.29 $\pm$ 1.29	35.26 $\pm$ 0.99
GSURE	36.80 $\pm$ 1.04	31.10 $\pm$ 1.40	33.68 $\pm$ 1.04
K-MSE	35.29 $\pm$ 1.12	31.67 $\pm$ 0.76	33.16 $\pm$ 1.04
SSDU	35.46 $\pm$ 1.03	33.48 $\pm$ 0.71	33.92 $\pm$ 1.15
LDAMP-SURE	34.97 $\pm$ 1.23	33.56 $\pm$ 1.39	32.87 $\pm$ 1.43
ENSURE	37.36 $\pm$ 0.92	34.13 $\pm$ 0.90	34.98 $\pm$ 0.93
	Structural Similarity Index (SSIM)		
	4x	4x, $\sigma = 0.03$	6x
E-to-E-Sup	0.97 $\pm$ 0.00	0.95 $\pm$ 0.01	0.94 $\pm$ 0.01
L-by-L- Sup	0.95 $\pm$ 0.00	0.95 $\pm$ 0.00	0.94 $\pm$ 0.00
GSURE	0.93 $\pm$ 0.01	0.91 $\pm$ 0.01	0.92 $\pm$ 0.02
K-MSE	0.95 $\pm$ 0.01	0.86 $\pm$ 0.02	0.93 $\pm$ 0.01
SSDU	0.93 $\pm$ 0.02	0.88 $\pm$ 0.04	0.92 $\pm$ 0.01
LDAMP-SURE	0.96 $\pm$ 0.00	0.94 $\pm$ 0.01	0.93 $\pm$ 0.01
ENSURE	0.97 $\pm$ 0.00	0.93 $\pm$ 0.01	0.94 $\pm$ 0.01

use of the data term alone will result in over-fitting, similar to observations in DIP methods as the number of epochs increase. The divergence term may be viewed as a network regularization, which serves to minimize noise amplification.

#### D. Network details

All the experiments utilized a model-based deep learning architecture, as shown in Fig. 2. The CNN had five layers, each with  $3 \times 3$  convolution, batch normalization, and ReLU non-linearity. Fig. 2 also shows the number of feature maps on top of each layer. The network had shared parameters in three unrolling steps. We trained the network for a total of fifty epochs with a fixed learning rate of  $10^{-3}$ . The data-consistency (DC) step utilized the complex data, whereas the CNN used the real and imaginary components of the complex data as channels.

## IV. RESULTS

We consider publicly available [6] parallel MRI brain data acquired using a 3-D T2 CUBE sequence with Cartesian

readouts using a 12-channel head coil at the University of Iowa on a 3T GE MR750w scanner. The Institutional Review Board at the University of Iowa approved the data acquisition, and written consent was obtained from the subjects. The matrix dimensions were  $256 \times 232 \times 208$  with a 1 mm isotropic resolution. Fully sampled multi-channel brain images of nine volunteers were collected, out of which data from five subjects were used for training. The data from two subjects were used for testing and the remaining two for validation. We utilized the ESPIRiT algorithm [31] to estimate the coil sensitivity maps.

#### A. Comparison with state-of-the-art methods

We compare the proposed ENSURE approach with the following supervised and unsupervised methods.

**Two supervised learning algorithms** E-to-E-Sup and L-by-L-Sup: The E-to-E-Sup approach refers to the end-to-end supervised training approach [6]. To make it consistent with the rest of the experiments, we use multiple sampling patterns during training. The L-by-L-Sup uses a similar acquisition and reconstruction architecture but relies on the supervised training of the CNNs in each layer. Both approaches use the loss function in (4) for training. We note that the number of free parameters in L-by-L-Sup is threefold higher than E-to-E-Sup, where the CNN parameters are shared across iterations. **GSURE-based unsupervised learning:** The GSURE loss, which is an unbiased estimate of projected MSE in (8), was originally introduced for regularization parameter selection. We consider the direct use of GSURE to train deep image reconstruction algorithms. Here, the sampling operator is assumed to be the same for all training images as considered in [19].

**Unsupervised learning with different sampling patterns:** We compare the proposed scheme against K-MSE, SSDU [25], and LDAMP-SURE [19]. The measurement operators are assumed to be different for each image in all of these approaches. The K-MSE (7) loss function involves the square of the error between measured and predicted k-space. As discussed previously, the K-MSE approach is vulnerable to over-fitting to noise. To minimize over-fitting, SSDU partitions the measured k-space samples into two disjoint groups: one group is used to reconstruct the images, while the second is used to evaluate the loss function. The 80-20 partition of k-space offered the best PSNR in our experimental setup. The LDAMP-SURE algorithm relies on layer-by-layer training. The five-layer CNN at each layer is independently trained as a denoiser using the SURE loss function.

We consider the recovery from 2-D random sampled multi-channel data in Table I. The peak signal to noise ratio (PSNR) and structural similarity index (SSIM) [32] for two different acceleration factors of 4x and 6x are reported in the first and last columns. To study the impact of measurement noise on the algorithms, we also consider a setting with additional Gaussian noise of standard deviation  $\sigma = 0.03$  added to the undersampled k-space data at 4x acceleration; these results are shown in the second column of Table I. The top two rows consider the supervised setting, while the remaining rows denote the unsupervised methods discussed above.

Fig. 3 visually compares the reconstruction quality of different unsupervised learning techniques with E-2-E-Sup learning at the 4x acceleration factor. In this low-noise setting, K-MSE offers nearly the same reconstruction quality as SSDU, which is also seen in Table I. The zoomed region shows that LDAMP-SURE, K-MSE, and SSDU have visible artifacts in the reconstructions compared to GSURE and ENSURE. The image quality of GSURE and ENSURE are comparable in this setting.

Fig. 4 shows reconstruction results at a higher acceleration factor of 6x. We note that the performance of the ENSURE approach is comparable to that of the supervised approach at this high acceleration rate. By contrast, we observe that GSURE, K-MSE, and LDAMP-SURE exhibit more noise-like artifacts along with blurring. A green rectangle in the zoomed images shows a hallucinated feature in the LDAMP-SURE because of layer-by-layer training of individual networks instead of end-to-end training in the proposed ENSURE approach. The SSDU approach offers less-noisy reconstructions compared to these approaches. However, the PSNR is around 0.5 dB lower than ENSURE. An arrow in the zoomed cerebellum region points to a feature that is well preserved by ENSURE while blurred by SSDU.

The original k-space data was already corrupted by noise. Because the algorithms are designed to overcome the impact of noise, we compare the performance in the higher noise setting in Fig. 5, which can also be seen in the second column of Table I. We added Gaussian noise of standard deviation  $\sigma = 0.03$  to the measured k-space data at 4x acceleration. In this setting, we observe that E-to-E-Sup and L-to-L-Sup have nearly the same mean PSNR values. We observe that the LDAMP-SURE approach performs better than the GSURE approach in this high noise setting, as reported in [19]. In particular, the projected MSE is a poor approximation for the MSE, which translates to poor reconstructions in the presence of noise. The improved performance of SSDU over KMSE shows that the partitioning strategy used in SSDU can reduce the over-fitting to noise. The ENSURE approach offers the best PSNR out of the unsupervised strategies and is comparable in PSNR and image quality to E-to-E-Sup.

### B. Impact of the different components of ENSURE loss

The ENSURE approach has two key differences from the GSURE framework: (a) the use of an ensemble of sampling patterns, and (b) the use of additional weighting within the data consistency term. We now study the impact of these components on performance.

1) *Need for using an ensemble of measurement operators:* We compare the GSURE framework, which uses a single sampling pattern for all the images, with the ENSURE formulation, which uses multiple sampling operators in Figure 6. A one-dimensional Cartesian sampling at 2x acceleration with an additional Gaussian noise of  $\sigma = 0.02$  was used. We note that aliasing artifacts and blurring are visible in the GSURE approach. In contrast, the ENSURE approach offers comparable performance to the E-to-E-Sup-MSE. A major source of the improved performance is the use of the ensemble

of measurement operators, which makes ENSURE closely approximate the true MSE. By contrast, the GSURE approach is only approximating the projected MSE, which is inferior in the undersampled setting, as discussed in [19].

2) *Impact of the weighting:* This experiment compares the impact of the proposed weighting strategy in (13) at 4x acceleration using a 2D random variable-density sampling pattern. We trained two networks with experimental setups that are similar except for the loss function. When we set the weights  $\mathbf{W}$  to identity in (14), it results in a network trained with the ENSURE loss without weighting. The reconstruction quality and error maps in Fig. 7 demonstrate that the proposed weighting scheme improves the reconstruction quality significantly.

## V. DISCUSSION

We observe from Table I, as well as the figures, that the proposed unsupervised learning using the ENSURE loss function offers PSNR and SSIM values that are comparable to those of E-to-E-Sup. The experiments in Section IV-B show that the ensemble of measurement operators and the weighted loss function enabled the ENSURE loss to closely approximate the true MSE when fully sampled and noise-free images are not available.

We note that the performance of the L-by-L-Sup approach, which has threefold more parameters, is only marginally worse than the E-to-E-Sup approach in all the settings. We note that the LDAMP-SURE approach, which relies on layer-by-layer training, is worse than ENSURE. This deterioration in performance may be attributed to the non-Gaussianity of the alias artifacts at each iteration, which is the key assumption used in LDAMP-SURE. We observe that the K-MSE scheme offers low performance, especially at high noise and highly accelerated settings. This is caused by the over-fitting of the network to the noise within the measurements. The partitioning strategy used in SSDU is observed to offer improved performance over K-MSE, especially in the high noise setting. Similarly, the performance improvement of ENSURE over GSURE is more significant in the high noise and highly accelerated setting.

The ENSURE and GSURE techniques depend on the estimation of noise variance in the measured data. In this work, we found it experimentally using trial and error. We estimated the noise variance for LDAMP-SURE implementation as suggested in [21]. However, it is possible to estimate the noise variance from noisy data itself. LDAMP-SURE [19], [21] unrolls the approximate message passing (AMP) [33] algorithm, which estimates noise in the intermediate reconstruction. Another possibility could be to use a variance estimation strategy such as [34], [35]. Zhussip [21] suggests another heuristic to estimate noise standard deviation that utilizes only the real part of complex data.

In this work, we used the network architecture shown in Fig. 2. However, we note that any direct-inversion or model-based network architecture can use the proposed ENSURE loss function. Unlike LDAMP-SURE, our proposed method does not depend on the unrolling of any specific algorithm.

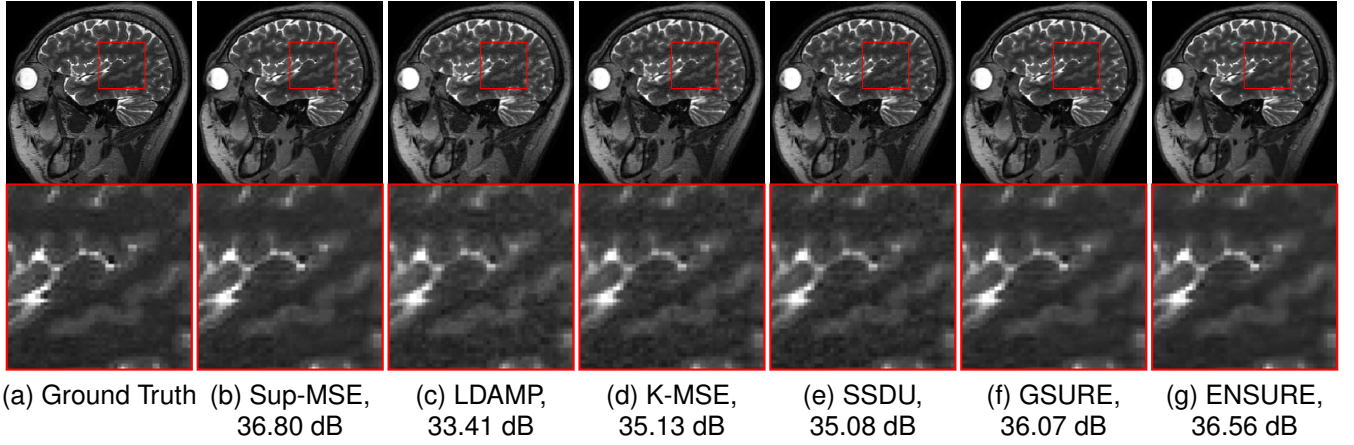


**Fig. 3.** This figure compares reconstruction results at 4x acceleration on a test slice. We can observe from the zoomed region that the proposed ENSURE approach results in comparable reconstruction quality to that of supervised training with MSE (Sup-MSE). Here, LDAMP refers to the LDAMP-SURE algorithm.

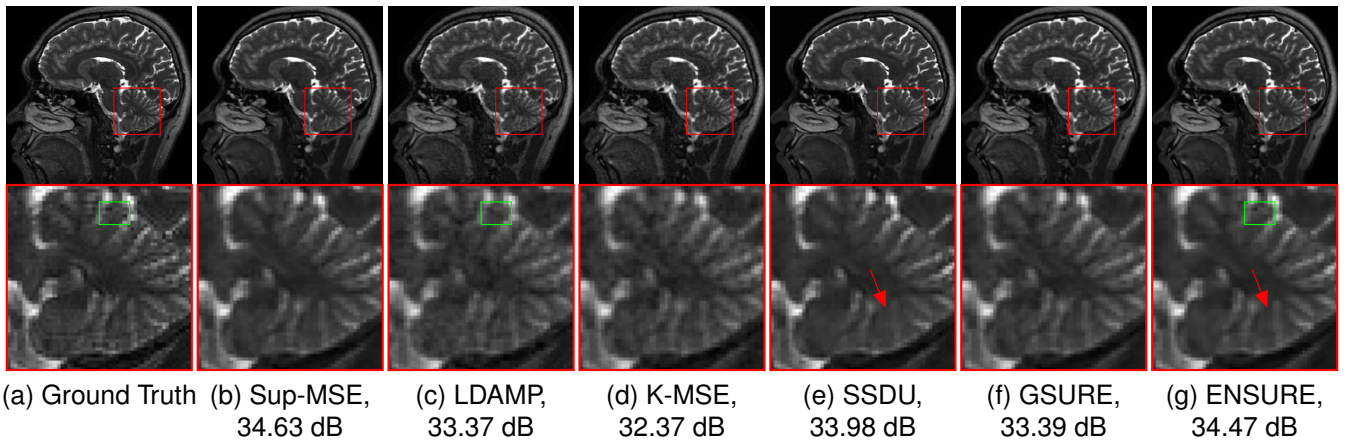


**Fig. 4.** Reconstruction results at a higher acceleration factor of 6x. We observe that, even at this high acceleration, the proposed ENSURE approach results in similar quantitative and qualitative reconstruction quality to that of supervised MSE training. The arrow in the zoomed region points to a feature well captured using ENSURE as compared to SSDU.

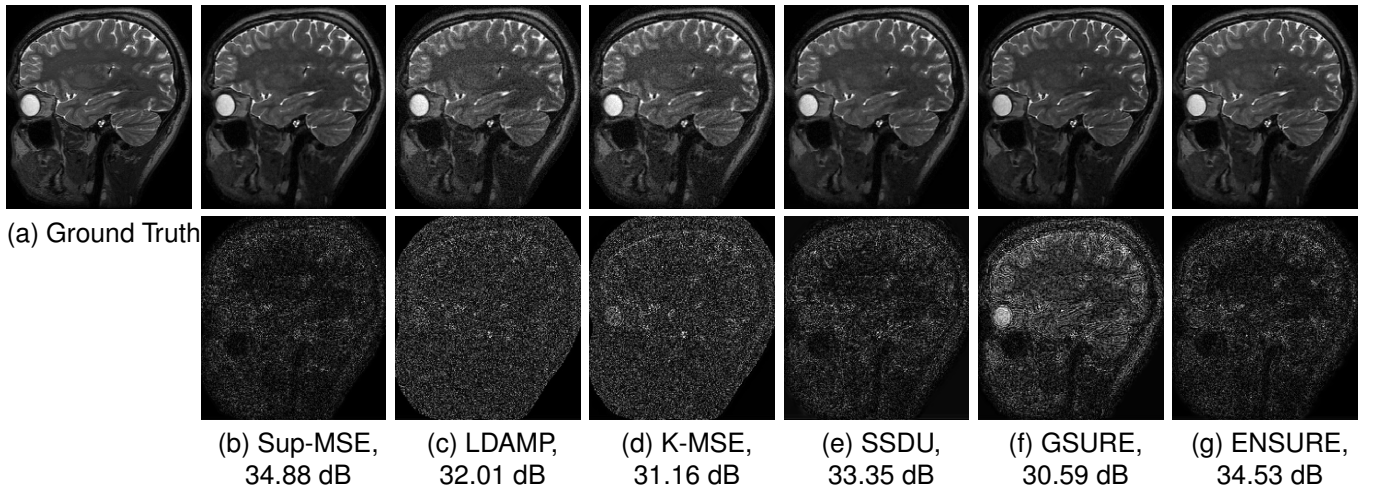


**Fig. 5.** Reconstruction results at 4x acceleration with added Gaussian noise of  $\sigma = 0.03$  in the measurements. The bottom row shows the corresponding error maps. We observe that ENSURE is robust to noise changes compared to other algorithms due to the use of a divergence term that we can interpret as a regularization term. The magnitude of error images is multiplied by 4 for visualization purposes.



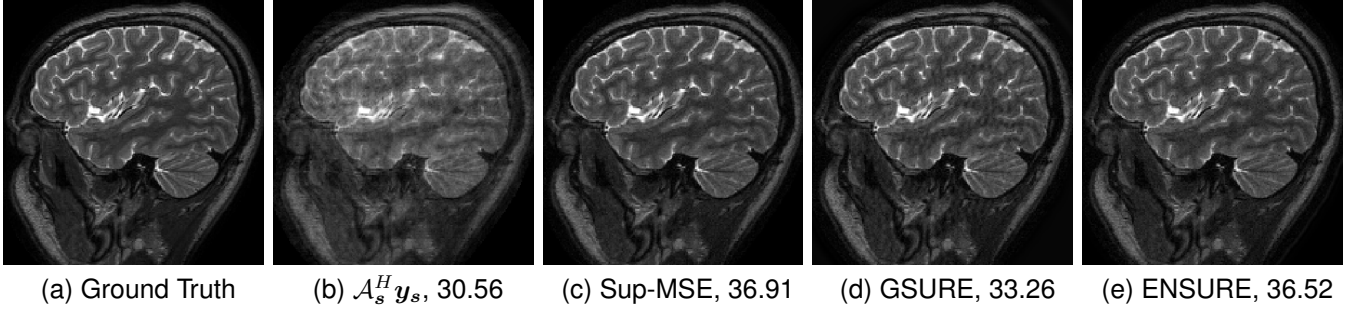


Fig. 6. This example demonstrates the benefit of sampling an image with multiple measurement operators in the one-dimensional sampling case at a 2X acceleration factor with added Gaussian noise of  $\sigma = 0.02$ . The numbers in the sub-captions show PSNR (dB) values.

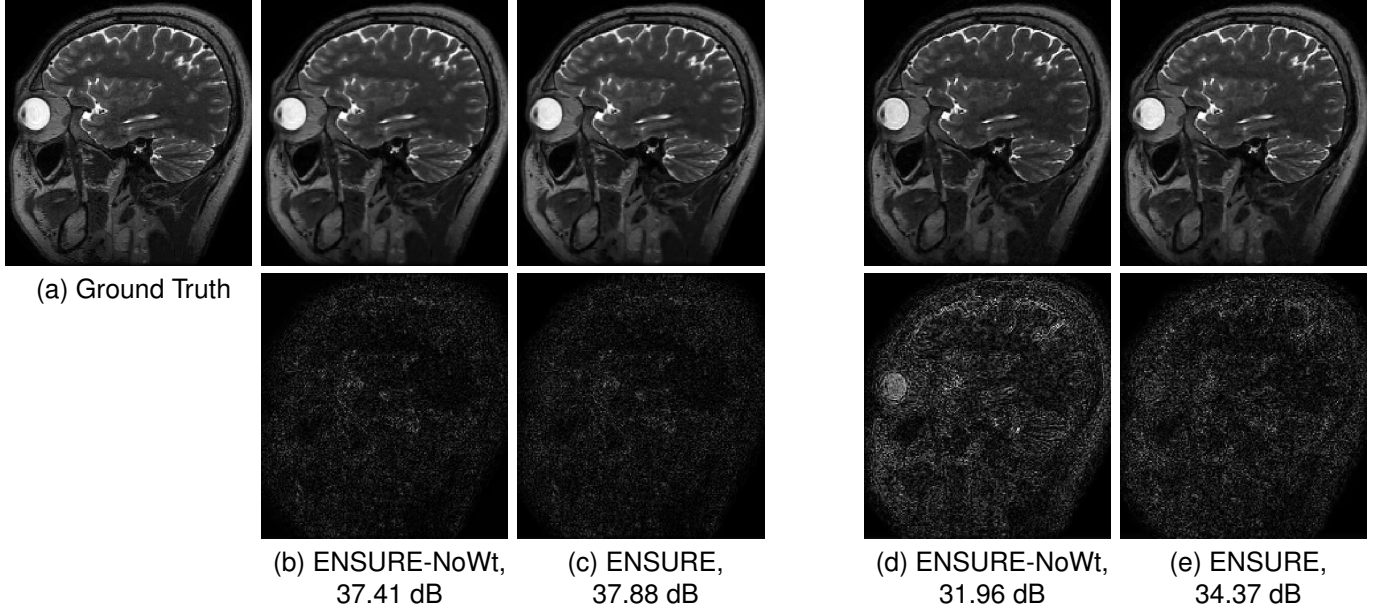


Fig. 7. This figure shows the benefit of the proposed weighting strategy. It visually compares the reconstruction quality of ENSURE with and without the proposed weighting scheme. The magnitude of error images is multiplied by 4 for visualization purposes. (b) and (c) refer to the case when no simulated noise is added to the measurements. (d) and (e) refer to the experimental setup when we added Gaussian noise of  $\sigma = 0.03$  to the measurements.

The use of more sophisticated network architecture, together with larger datasets, may offer further improved performance.

The SSDU method [25] suggests partitioning the measured k-space into 60-40 such that 60% is used in the DC step and 40% in the loss function estimation. With our dataset and network architecture, we experimented with several different partitions of the k-space, including the suggested 60-40 split, and found that an 80-20 division performed best.

## VI. CONCLUSIONS

We introduced a novel loss function for the unsupervised training of deep-learning-based image reconstruction algorithms when fully sampled training data is not available. The proposed approach is the extension of the generalized SURE (GSURE) approach. The key distinction of the framework from GSURE is the use of an ensemble of measurement operators. In particular, we assume that different images are measured by different sampling operators. Our theoretical results show that the proposed ENSURE loss function

closely approximates the true MSE without requiring the fully sampled images. More specifically, the use of the different sampling operators enables us to obtain a better approximation of the loss than GSURE, which approximates the projected MSE; the MSE of the projections of the images to the range space of the measurement operator is a poor approximation of the true MSE, especially in highly undersampled settings. The experiments confirm that the deep learning networks trained using the ENSURE approach without fully sampled training data closely resemble the networks trained using a supervised loss function. While our focus in this work was on an MRI reconstruction problem, this approach is broadly applicable to general inverse problems, including deblurring and tomography.

## APPENDIX

From (1), we note that  $\mathbf{u} = \mathcal{A}_s^H \mathbf{C}^{-1} \mathbf{y}_s$  is Gaussian distributed with mean  $\mathcal{A}_s^H \mathbf{C}^{-1} \mathcal{A}_s \boldsymbol{\rho}$  and covariance matrix  $\mathcal{A}_s^H \mathbf{C}^{-1} \mathcal{A}_s$ , i.e.,



$$p(\mathbf{u}|\boldsymbol{\rho}) = \mathcal{N}(\mathcal{A}_s^H \mathbf{C}^{-1} \mathcal{A}_s \boldsymbol{\rho}, \mathcal{A}_s^H \mathbf{C}^{-1} \mathcal{A}_s) \quad (20)$$

$$= q(\mathbf{u}) \exp(\boldsymbol{\rho}^T \mathbf{u} - g(\boldsymbol{\rho})). \quad (21)$$

Here,  $q(\mathbf{u})$  is independent of  $\boldsymbol{\rho}$ . Similarly,  $g(\boldsymbol{\rho})$  is dependent on  $\boldsymbol{\rho}$ , which is not often available, and is independent of  $\mathbf{u}$ :

$$q(\mathbf{u}) = K \exp\left[-\frac{1}{2} \mathbf{u}^H \left[\mathcal{A}_s^H \mathbf{C}^{-1} \mathcal{A}_s\right]^\dagger \mathbf{u}\right] \quad (22)$$

$$g(\boldsymbol{\rho}) = \frac{1}{2} \boldsymbol{\rho}^H \mathcal{A}_s^H \mathbf{C}^{-1} \mathcal{A}_s \boldsymbol{\rho} \quad (23)$$

Here,  $K$  is a constant. Expanding the loss in (13), we get

$$\mathcal{L} = \mathbb{E}_{\mathbf{u}} \mathbb{E}_{\mathbf{s}} \left[ \|\mathbf{W}_s \hat{\boldsymbol{\rho}}\|_2^2 \right] + \mathbb{E}_{\mathbf{u}} \mathbb{E}_{\mathbf{s}} \left[ \|\mathbf{W}_s \boldsymbol{\rho}\|_2^2 \right] - 2 \mathbb{E}_{\mathbf{u}} \mathbb{E}_{\mathbf{s}} \left[ \hat{\boldsymbol{\rho}}^T \mathbf{W}_s^T \mathbf{W}_s \boldsymbol{\rho} \right] \quad (24)$$

Our goal is to minimize the above expression with respect to  $\hat{\boldsymbol{\rho}}$ . We note that the first term is independent of  $\boldsymbol{\rho}$ , while the second term is independent of  $\boldsymbol{\rho}$  and can be viewed as a constant while minimizing with respect to  $\hat{\boldsymbol{\rho}}$ . We will now focus on the third term, which includes both  $\boldsymbol{\rho}$  and  $\hat{\boldsymbol{\rho}}$ , and estimate it using SURE. Denoting  $\mathbf{D} = \mathbf{W}_s^T \mathbf{W}_s$ , the last term in (24) is

$$\mathbb{E}_{\mathbf{u}} \left[ \hat{\boldsymbol{\rho}}^T \mathbf{D} \boldsymbol{\rho} \right] = \int_{-\infty}^{+\infty} \hat{\boldsymbol{\rho}}^T \mathbf{D} \boldsymbol{\rho} \underbrace{q(\mathbf{u}) \exp(\boldsymbol{\rho}^T \mathbf{u} - g(\boldsymbol{\rho}))}_{p(\mathbf{u})} d\mathbf{u}$$

Let  $h(\mathbf{u}) = \exp(\boldsymbol{\rho}^T \mathbf{u} - g(\boldsymbol{\rho}))$ , then  $\nabla_{\mathbf{u}} h(\mathbf{u}) = \boldsymbol{\rho} h(\mathbf{u})$ . Substituting for  $\boldsymbol{\rho} h(\mathbf{u})$ , we obtain

$$\begin{aligned} \mathbb{E}_{\mathbf{u}} \left[ \hat{\boldsymbol{\rho}}^T \mathbf{D} \boldsymbol{\rho} \right] &= \int_{-\infty}^{+\infty} \hat{\boldsymbol{\rho}}^T \mathbf{D} q(\mathbf{u}_s) \nabla_{\mathbf{u}} h(\mathbf{u}) d\mathbf{u} \\ &= \langle q(\mathbf{u}) \mathbf{D} \hat{\boldsymbol{\rho}}, \nabla_{\mathbf{u}} h(\mathbf{u}) \rangle \\ &= - \left\langle h(\mathbf{u}), \nabla_{\mathbf{u}} \cdot [q(\mathbf{u}) \mathbf{D} \hat{\boldsymbol{\rho}}] \right\rangle \end{aligned}$$

Expanding the second term in the inner-product using the chain rule, we obtain

$$\begin{aligned} \nabla_{\mathbf{u}} \cdot [q(\mathbf{u}) \mathbf{D} \hat{\boldsymbol{\rho}}] &= q(\mathbf{u}) \nabla_{\mathbf{u}} \cdot \mathbf{D} \hat{\boldsymbol{\rho}} + \mathbf{D} \hat{\boldsymbol{\rho}} \cdot \nabla_{\mathbf{u}} q(\mathbf{u}) \\ &= q(\mathbf{u}) \left( \nabla_{\mathbf{u}} \cdot \mathbf{D} \hat{\boldsymbol{\rho}} + \mathbf{D} \hat{\boldsymbol{\rho}} \cdot \frac{\nabla_{\mathbf{u}} q(\mathbf{u})}{q(\mathbf{u})} \right) \\ &= q(\mathbf{u}) \left( \nabla_{\mathbf{u}} \cdot \mathbf{D} \hat{\boldsymbol{\rho}} + \mathbf{D} \hat{\boldsymbol{\rho}} \cdot \underbrace{\frac{\nabla_{\mathbf{u}} \ln q(\mathbf{u})}{-1}}_{-\boldsymbol{\rho}_{\text{LS}}} \right) \end{aligned}$$

In the last step, we used the property

$$-\nabla_{\mathbf{u}} \ln q(\mathbf{u}) = \left[ \mathcal{A}_s^H \mathbf{C}^{-1} \mathcal{A}_s \right]^\dagger \mathcal{A}_s^H \mathbf{C}^{-1} \mathbf{y}_s = \boldsymbol{\rho}_{\text{LS}} \quad (25)$$

Because  $q(\mathbf{u}) h(\mathbf{u}) = p(\mathbf{u})$ , we obtain

$$\mathbb{E}_{\mathbf{u}} \left[ \hat{\boldsymbol{\rho}}^T \mathbf{D} \boldsymbol{\rho} \right] = -\mathbb{E}_{\mathbf{u}} \left[ \nabla_{\mathbf{u}} \cdot \mathbf{D} \hat{\boldsymbol{\rho}} \right] + \mathbb{E}_{\mathbf{u}} \left[ \hat{\boldsymbol{\rho}}^T \mathbf{D} \boldsymbol{\rho}_{\text{LS}} \right]$$

Substituting this in (24), we obtain

$$\begin{aligned} \mathcal{L} &= \mathbb{E}_{\mathbf{u}} \mathbb{E}_{\mathbf{s}} \left[ \|\mathbf{W}_s \hat{\boldsymbol{\rho}}\|_2^2 \right] + \mathbb{E}_{\mathbf{u}} \mathbb{E}_{\mathbf{s}} \left[ \|\mathbf{W}_s \boldsymbol{\rho}\|_2^2 \right] \\ &\quad - 2 \mathbb{E}_{\mathbf{u}} \mathbb{E}_{\mathbf{s}} \left[ \hat{\boldsymbol{\rho}}^T \mathbf{D} \boldsymbol{\rho}_{\text{LS}} - \nabla_{\mathbf{u}} \cdot \mathbf{D} \hat{\boldsymbol{\rho}} \right] \end{aligned} \quad (26)$$

Combining the first and third terms, we obtain the ENSURE loss as

$$\begin{aligned} \mathcal{L} &= \mathbb{E}_{\mathbf{u}} \mathbb{E}_{\mathbf{s}} \left[ \|\mathbf{W}_s(\hat{\boldsymbol{\rho}} - \boldsymbol{\rho}_{\text{LS}})\|_2^2 \right] \\ &\quad + 2 \mathbb{E}_{\mathbf{u}} \mathbb{E}_{\mathbf{s}} \left[ \nabla_{\mathbf{u}} \cdot \mathbf{W}_s^T \mathbf{W}_s \hat{\boldsymbol{\rho}} \right] + S \end{aligned} \quad (27)$$

Here,  $S = \mathbb{E}_{\mathbf{u}} \mathbb{E}_{\mathbf{s}} \left[ \|\mathbf{W}_s \boldsymbol{\rho}\|_2^2 - \|\mathbf{W}_s \boldsymbol{\rho}_{\text{LS}}\|_2^2 \right]$  is a constant that is independent of the network.

## REFERENCES

- [1] M. Lustig, D. L. Donoho, J. M. Santos *et al.*, "Compressed sensing MRI," *IEEE Signal Process. Mag.*, vol. 25, no. 2, p. 72, 2008.
- [2] E. Candes and J. Romberg, "Sparsity And Incoherence In Compressive Sampling," *Inverse Probl.*, vol. 23, no. 3, p. 969, 2007.
- [3] J. A. Fessler, "Model-Based Image Reconstruction for MRI," *IEEE Signal Process. Mag.*, vol. 27, no. 4, pp. 81–89, 2010.
- [4] H. Chen, Y. Zhang, M. K. Kalra *et al.*, "Low-Dose CT with a Residual Encoder-Decoder Convolutional Neural Network," *IEEE Trans. Med. Imag.*, vol. 36, no. 12, pp. 2524–2535, 2017.
- [5] Y. Han, L. Sunwoo, and J. C. Ye, "k-space deep learning for accelerated MRI," *IEEE Trans. Med. Imag.*, 2019.
- [6] H. K. Aggarwal, M. P. Mani, and M. Jacob, "MoDL: Model Based Deep Learning Architecture for Inverse Problems," *IEEE Trans. Med. Imag.*, vol. 38, no. 2, pp. 394–405, 2019.
- [7] Y. Yang, J. Sun, H. Li *et al.*, "Deep ADMM-Net for Compressive Sensing MRI," in *Advances in Neural Information Processing Systems* 29, 2016, pp. 10–18.
- [8] J. Adler and O. Öktem, "Learned primal-dual reconstruction," *IEEE Trans. Med. Imag.*, vol. 37, no. 6, pp. 1322–1332, 2018.
- [9] K. Hammernik, T. Klatzer, E. Kobler *et al.*, "Learning a Variational Network for Reconstruction of Accelerated MRI Data," *Magnetic resonance in Medicine*, vol. 79, no. 6, pp. 3055–3071, 2017.
- [10] L. Zhang and W. Zuo, "Image Restoration: From Sparse and Low-Rank Priors to Deep Priors," *IEEE Signal Process. Mag.*, vol. 34, no. 5, pp. 172–179, 2017.
- [11] G. Yang, S. Yu, H. Dong *et al.*, "DAGAN: Deep De-Aliasing Generative Adversarial Networks For Fast Compressed Sensing MRI Reconstruction," *IEEE Trans. Med. Imag.*, vol. 37, no. 6, pp. 1310–1321, 2017.
- [12] J. Zbontar, F. Knoll, A. Sriram *et al.*, "fastMRI: An open dataset and benchmarks for accelerated MRI," *arXiv preprint arXiv:1811.08839*, 2018.
- [13] P. C. Hansen and D. P. O'Leary, "The Use Of The L-Curve In The Regularization Of Discrete Ill-Posed Problems," *SIAM journal on scientific computing*, vol. 14, no. 6, pp. 1487–1503, 1993.
- [14] G. H. Golub, M. Heath, and G. Wahba, "Generalized Cross-Validation As a Method For Choosing a Good Ridge Parameter," *Technometrics*, vol. 21, no. 2, pp. 215–223, 1979.
- [15] C. M. Stein, "Estimation Of The Mean Of A Multivariate Normal Distribution," *The annals of Statistics*, pp. 1135–1151, 1981.
- [16] D. L. Donoho and I. M. Johnstone, "Adapting To Unknown Smoothness Via Wavelet Shrinkage," *Journal of the American Statistical Association*, vol. 90, no. 432, pp. 1200–1224, 1995.
- [17] T. Blu and F. Luisier, "The SURE-LET Approach To Image Denoising," *IEEE Trans. Image Process.*, vol. 16, no. 11, pp. 2778–2786, 2007.
- [18] F. Luisier, C. Vonesch, T. Blu *et al.*, "Fast Interscale Wavelet Denoising Of Poisson-Corrupted Images," *Signal processing*, vol. 90, no. 2, pp. 415–427, 2010.
- [19] C. A. Metzler, A. Mousavi, R. Heckel *et al.*, "Unsupervised Learning with Stein's Unbiased Risk Estimator," *arXiv preprint arXiv:1805.10531*, 2018.
- [20] M. Zhussip, S. Soltanayev, and S. Y. Chun, "Extending Stein's Unbiased Risk Estimator to Train Deep Denoisers with Correlated pPairs of Noisy Images," in *Advances in Neural Information Processing Systems*, 2019.
- [21] M. Zhussip, S. Soltanayev, and S. Y. Chun, "Training deep learning based image denoisers from undersampled measurements without ground truth and without image prior," in *IEEE/CVF Conference on Computer Vision and Pattern Recognition*, 2019, pp. 10 255–10 264.
- [22] J. Lehtinen, J. Munkberg, J. Hasselgren *et al.*, "Noise2Noise: Learning Image Restoration without Clean Data," in *International Conference on Machine Learning*, 2018, pp. 2965–2974.
- [23] A. Krull, T.-O. Buchholz, and F. Jug, "Noise2Void-Learning Denoising From Single Noisy Images," in *IEEE Conference on Computer Vision and Pattern Recognition*, 2019, pp. 2129–2137.

- [24] Y. C. Eldar, "Generalized SURE for Exponential Families: Applications to Regularization," *IEEE Trans. Signal Process.*, vol. 57, no. 2, pp. 471–481, 2008.
- [25] B. Yaman, S. A. H. Hosseini, S. Moeller *et al.*, "Self-Supervised Learning Of Physics-Guided Reconstruction Neural Networks Without Fully Sampled Reference Data," *Magn. Reson. Med.*, pp. 3172–3191, 2020.
- [26] E. Cha, H. Chung, E. Y. Kim *et al.*, "Unpaired Training of Deep Learning tMRA for Flexible Spatio-Temporal Resolution," *IEEE Trans. Med. Imag.*, vol. 40, no. 1, pp. 166–179, 2020.
- [27] D. Ulyanov, A. Vedaldi, and V. Lempitsky, "Deep Image Prior," in *IEEE Conference on Computer Vision and Pattern Recognition*, 2018, pp. 9446–9454.
- [28] A. Krull, T. Vičar, M. Prakash *et al.*, "Probabilistic Noise2Void: Un-supervised Content-Aware Denoising," *Frontiers in Computer Science*, vol. 2, p. 5, 2020.
- [29] S. Ramani, T. Blu, and M. Unser, "Monte-Carlo SURE: A Black-Box Optimization Of Regularization Parameters For General Denoising Algorithms," *IEEE Trans. Image Process.*, vol. 17, no. 9, pp. 1540–1554, 2008.
- [30] K. P. Pruessmann, M. Weiger, M. B. Scheidegger *et al.*, "SENSE: Sensitivity encoding for fast MRI," *Magnetic Resonance in Medicine*, vol. 42, no. 5, pp. 952–962, 1999.
- [31] M. Uecker, P. Lai, M. J. Murphy *et al.*, "ESPIRiT - An eigenvalue approach to autocalibrating parallel MRI: Where SENSE meets GRAPPA," *Magnetic Resonance in Medicine*, vol. 71, no. 3, pp. 990–1001, 2014.
- [32] Z. Wang, A. C. Bovik, H. R. Sheikh *et al.*, "Image Quality Assessment: From Error Visibility To Structural Similarity," *IEEE Trans. Image Process.*, vol. 13, no. 4, pp. 600–612, 2004.
- [33] S. Rangan, P. Schniter, and A. K. Fletcher, "Vector approximate message passing," *IEEE Trans. Inf. Theory*, vol. 65, no. 10, pp. 6664–6684, 2019.
- [34] D. L. Donoho and J. M. Johnstone, "Ideal Spatial Adaptation By Wavelet Shrinkage," *Biometrika*, vol. 81, no. 3, pp. 425–455, 1994.
- [35] M. Hashemi and S. Beheshti, "Adaptive noise variance estimation in BayesShrink," *IEEE Signal Processing Letters*, vol. 17, no. 1, pp. 12–15, 2009.